Journal of Sound and Vibration 332 (2013) 17–32

Contents lists available at SciVerse ScienceDirect

Journal of Sound and Vibration

journal homepage: www.elsevier.com/locate/jsvi

Integrated optimization of actuator placement and vibration control for piezoelectric adaptive trusses

W.P. Li*, H. Huang

School of Astronautics, BEIHANG University, Beijing 100191, PR China

ARTICLE INFO

Article history:
Received 15 September 2011
Received in revised form
12 June 2012
Accepted 9 August 2012
Handling Editor: J. Lam
Available online 11 September 2012

ABSTRACT

In this paper, the integrated optimization of actuator placement and vibration control for piezoelectric adaptive truss is studied. Based on the dynamic finite element (FE) model and a linear-quadratic-Gaussian (LQG) model of vibration control for an adaptive truss, an integrated optimization model is built in which an improved quadratic performance index is adopted as the objective function and the mode closed-loop damping ratio, modal controllability and actuator number are selected as the constraints. A layered optimization strategy is implemented to address this optimization problem with discrete-continuous design variable. To prevent the optimization process from converging to the local optimal solution, the genetic algorithm (GA) for outside-layer optimization is extended with an improved penalty function. Numerical examples and the vibration control experiments for piezoelectric adaptive truss were used to validate the efficiency of the proposed method. The following conclusions were drawn from the results. (1) The improved penalty function can orient the optimization process to the global optimal solution. (2) Although the number of struts on the truss is large, the optimization computation time is short because of the high efficiency of the proposed method. (3) In the experiment, the quadratic performance index, modal response and sensor signals for the present paper's optimal actuator placement scheme are better than those described in the literature, but the placement requires more energy, which is consistent with the numerical results.

1. Introduction

The main structures of many spacecrafts, such as the International Space Station, space-deployable antennas and reflectors, and space-based interferometers, are large truss-type structures. They are lightweight and flexible and have little inherent damping and low-frequency fundamental modes. Onboard disturbances caused by activities such as orbital maneuvers, docking and thermal gradients can easily excite structure vibration. The structure vibration must be effectively suppressed to meet stringent requirements for vibration-sensitive missions. One promising method to address this issue is to use the technology of adaptive structures, which employs embedded actuators, sensors, and microprocessors to analyze the sensors' signals and to apply localized strains to ensure that the structure responds in the desired fashion [1–4].

Because of the complexity of the adaptive structure, the structure and control system is coupled. For instance, the vibration controller's coefficients are strongly dependent on the placement and orientation of the actuators/sensors, which

* Corresponding author. Tel.: +86 10 82339104.
E-mail address: Liweipeng@buaa.edu.cn (W.P. Li).

0022-460X/$ - see front matter © 2012 Elsevier Ltd. All rights reserved.
http://dx.doi.org/10.1016/j.jsv.2012.08.005

determine the effectiveness of structural vibration control. Therefore, researching the structure and control of integrated optimization strategies for adaptive structures is theoretically and practically significant. There has been much work published on intelligent structure integrated optimization. In terms of optimization strategy, Manning [5] proposed a two-stage optimization strategy for active member placement and strut cross-section and compensator parameter optimization for intelligent trusses. Gao [6] investigated integrated optimization of the actuator location and feedback gain in PZT smart trusses with stochastic structural parameters using a two-step optimization strategy. Xian [7] combined a layered strategy and an approximation concept, and formed a two-level, branched, multipoint approximation strategy for adaptive truss actuator placement optimization. Liu [8] took a two-level optimization method based on a simulated annealing algorithm to determine the optimal channel distribution and the optimal channel voltage for dynamic shape control of structures using piezoelectric materials. While, in terms of optimization method, Rao et al. [9] studied a game theory approach for actively controlling truss structural parameters and for controller integrated design. Xu et al. [10] presented a nonlinear programming method for determining the placement and gain of actuators and sensors in output feedback control systems. Zhao et al. [11] used a sequential linear programming algorithm to optimize piezoelectric intelligent truss structural elements and vibration controller gains simultaneously. Yang et al. [12] adopted an integer-real encoded genetic algorithm (GA) for integrated optimization of PZT smart-beam sensor/actuator placement/size and the controller gains. Xu et al. [13] discussed some issues associated with integrated optimization of structural topology, the number and placement of actuators and control parameters for piezoelectric smart trusses; some optimal strategies based on genetic algorithms were adopted in their study. Honda et al. [14] employed the placement of piezoelectric actuators, the lay-up configurations of laminated composite plates, and the H_2 vibration control system as design variables and optimized them simultaneously by GA. Dutta et al. [15] considered artificial bee colony and glowworm swarm optimization algorithms, to find the optimal locations of actuators/sensors and feedback gains of a cantilevered beam. The aforementioned research efforts show that a layered optimization strategy is effective for dealing with actuator placement and continuous variables (i.e., controller gains) mixed variables optimization, while GA is suitable for large-scale discrete variable optimization. However, almost all the efforts described in the literature only verify the optimization results with numerical examples, but no experiments. This is not enough for engineering applications.

In the present paper, actuator placement and vibration control integrated optimization for piezoelectric adaptive truss structures were studied. First, a dynamic model of adaptive truss and a LQG control model were built. Then an integrated optimization model of actuator placement and LQG controller, including discrete-continuous design variables, was proposed, and a layered optimization strategy was implemented. In addition, to prevent the optimization from converging to the local optimal solution, a GA applied to the outside-layer optimization was extended by introducing an improved penalty function. Optimization was conducted based on the mathematical model. To verify the validity of the results and promote engineering applications of this approach, experiments of vibration control for optimal actuator placement were conducted with a piezoelectric adaptive truss test-bed. Numerical calculations were also completed, and the experimental results were consistent with the numerical results.

2. Adaptive truss modeling

The dynamic FE model for an ordinary strut element and an active strut element are, respectively

$$\mathbf{F^e} = \mathbf{M^e}\ddot{\mathbf{U}}^{\mathbf{e}} + \mathbf{C_f^e}\dot{\mathbf{U}}^{\mathbf{e}} + \mathbf{K^e}\mathbf{U^e} \tag{1}$$

$$\mathbf{F^e} = \mathbf{M'^e}\ddot{\mathbf{U}}^{\mathbf{e}} + \mathbf{C_f'e}\dot{\mathbf{U}}^{\mathbf{e}} + \mathbf{K'^e}\mathbf{U^e} - \nu\mathbf{L_v^e} \tag{2}$$

where $\mathbf{F^e}$ and $\mathbf{U^e}$ are the load and displacement at the strut's ends. $\mathbf{M^e}(\mathbf{M'^e})$, $\mathbf{C_f^e}(\mathbf{C_f'e})$ and $\mathbf{K^e}(\mathbf{K'^e})$ are the mass, damping and stiffness matrix of ordinary strut elements (active strut elements), respectively. ν is the control voltage. $\mathbf{L_v^e}$ is the control force vector. With the Rayleigh damping assumption, $\mathbf{C_f^e}(\mathbf{C_f'e})$ can be expressed by the linear combination of $\mathbf{M^e}(\mathbf{M'^e})$ and $\mathbf{K^e}(\mathbf{K'^e})$.

By considering a nodal lumped mass, a piezoelectric adaptive truss dynamic FE model can be assembled as

$$\mathbf{F} + \mathbf{L_v}\mathbf{V} = M\ddot{\mathbf{U}} + \mathbf{C_f}\dot{\mathbf{U}} + \mathbf{K}\mathbf{U} \tag{3}$$

where $\mathbf{F}$ is the load vector. $\mathbf{M}$, $\mathbf{C_f}$ and $\mathbf{K}$ are the mass, damping and stiffness matrices of the structure, respectively. $\mathbf{U}$ is the nodal displacement vector. $\mathbf{L_v}$ is the sum of the $\mathbf{L_v^e}$ dimension expansion. $\mathbf{V}$ is the control voltage vector. In addition, the system's observation equation is

$$\mathbf{Y} = \mathbf{C_v}\mathbf{U} \tag{4}$$

In the present paper, LQG control is conducted using mode coordinates. Therefore, the mode coordinate vector $\mathbf{q}$ has a relationship with the modal displacement vector $\mathbf{U}$: $\mathbf{U} = \Phi \cdot \mathbf{q}$, where Φ is the modal matrix. Then the system decoupling dynamic equation and the observation equation for the mode coordinate can be derived from Eqs. (3) and (4)

$$\ddot{\mathbf{q}} + 2 \cdot \mathrm{diag}(\xi_i \omega_i) \cdot \dot{\mathbf{q}} + \mathrm{diag}(\omega_i^2) \cdot \mathbf{q} = \mathbf{\Phi^T}\mathbf{L_v}\mathbf{V} + \mathbf{\Phi^T}\mathbf{F} \tag{5}$$

$$\mathbf{Y} = \mathbf{C_v}\mathbf{\Phi}\mathbf{q} \tag{6}$$

where ω_i and ξ_i are the mode angular frequency and the mode damping coefficient, respectively.

3. LQG control modeling

3.1. LQG method

The LQG control method is applied for the vibration control of the adaptive truss. Accounting for system noise and with zero external loads (n_m-mode truncated), Eqs. (5) and (6) take the following forms in state space:

$$\dot{\mathbf{X}} = \mathbf{AX} + \mathbf{BV} + \mathbf{B_G w} \tag{7}$$

$$\mathbf{Y} = \mathbf{CX} + \mathbf{v} \tag{8}$$

where $\mathbf{A} = \begin{bmatrix} 0 & \mathbf{I} \\ -\mathrm{diag}(\omega_i^2) & -\mathrm{diag}(2\xi_i\omega_i) \end{bmatrix}$ $(i = 1,\ldots,n_m)$, $\mathbf{B} = \begin{bmatrix} \mathbf{0} & \mathbf{\Phi^T L_v} \end{bmatrix}^{\mathbf{T}}$, $\mathbf{C} = \begin{bmatrix} \mathbf{C_V \Phi} & \mathbf{0} \end{bmatrix}$ and $\mathbf{X} = \begin{bmatrix} \mathbf{q} & \dot{\mathbf{q}} \end{bmatrix}^{\mathbf{T}}$. $\mathbf{B_G}$ is a system noise input matrix. Control noise $\mathbf{w}$ and observation noise $\mathbf{v}$ are assumed to be zero-mean Gaussian processes and they are independent random variables, so they have the following covariances:

$$E(\mathbf{ww^T}) = \mathbf{W_k}, E(\mathbf{vv^T}) = \mathbf{V_k}, E(\mathbf{wv^T}) = \mathbf{0} \tag{9}$$

Here, assume $\mathbf{B_G} = \mathbf{B}$, $\mathbf{W_k} = 0.001 \cdot \mathbf{I}$, and $\mathbf{V_k} = 0.001 \cdot \mathbf{I}$.

According to linear-quadratic-regulator (LQR) theory, the quadratic performance index of the controlled structural response and the control energy are chosen to be the following objective function:

$$J = \frac{1}{2}\int_0^\infty (\mathbf{X^T Q X} + \mathbf{V^T R V})\, \mathrm{d}t \tag{10}$$

where $\mathbf{Q} = \begin{bmatrix} \mathrm{diag}(\omega_i^2) & 0 \\ 0 & \mathbf{I} \end{bmatrix}$ $(i = 1,\ldots,n_m)$ and $\mathbf{R} = r\mathbf{I}$ are semidefinite and definite weighted matrices, while the selection of weight factor r depended on balancing the importance of $\mathbf{X^T Q X}$ and $\mathbf{V^T R V}$.

Based on the minimal value principle, the optimal control gain is

$$\mathbf{G} = -\mathbf{R}^{-1}\mathbf{B}\mathbf{P_R} \tag{11}$$

where $\mathbf{P_R}$ is the solution of the following Riccati equation:

$$\mathbf{P_R A} + \mathbf{A^T P_R} + \mathbf{Q} - \mathbf{P_R B R^{-1} B^T P_R} = \mathbf{0} \tag{12}$$

Then the control voltage can be obtained as $\mathbf{V} = -\mathbf{G} \cdot \mathbf{X}$.

3.2. Observation function

Based on Kalman filter theory, the state-space equation of state variable estimation value for $\mathbf{X_e}$ is

$$\dot{\mathbf{X}}_\mathbf{e} = (\mathbf{A} - \mathbf{L_B C})\mathbf{X_e} + \begin{bmatrix} \mathbf{B} & \mathbf{L_B} \end{bmatrix} \begin{Bmatrix} \mathbf{V} \\ \mathbf{Y} \end{Bmatrix} \tag{13}$$

where $\mathbf{L_B} = \mathbf{P_K C^T V_k^{-1}}$. $\mathbf{P_K}$ can be obtained from the following Riccati equation:

$$\mathbf{A P_K} + \mathbf{P_K A^T} - \mathbf{P_K C^T V_K^{-1} C P_K} + \mathbf{B_G W_K B_G^T} = \mathbf{0} \tag{14}$$

3.3. Improvement of the objective function

As described in Eq. (10), a random system initial state will affect the value of J and therefore should be eliminated to ensure comparability in the following optimization. A new quadratic performance index $\bar{J}$ is defined

$$\bar{J} = \mathrm{tr}(\overline{\mathbf{P}}_\mathbf{o}) \tag{15}$$

where $\overline{\mathbf{P}}_\mathbf{o}$ is merely determined by the system structure and the controller coefficients and can be obtained from the following Lyapunov equation:

$$\overline{\mathbf{P}}_\mathbf{o}\mathbf{A_c} + \mathbf{A_c^T}\overline{\mathbf{P}}_\mathbf{o} + \mathbf{Q} + \mathbf{G^T R G} = \mathbf{0} \tag{16}$$

where $\mathbf{A_c} = \mathbf{A} - \mathbf{B} \cdot \mathbf{G}$.

3.4. Controllability equation

The control effect of the structural system is usually evaluated by mode controllability. Let $\overline{\mathbf{B}}$ denote line n_m+1 to $2n_m$ in $\mathbf{B}$. The element on the jth line and the ith column of $\overline{\mathbf{B}}$ is the force on the jth mode when a unit voltage is applied to the

ith actuator. Using paper [16]'s method, the jth mode controllability is as follows:

$$\tau_j = \overline{\mathbf{B}}_\mathbf{j}\overline{\mathbf{B}}_\mathbf{j}^\mathbf{T}, \quad j = 1,\ldots,n_m \tag{17}$$

where $\overline{\mathbf{B}}_\mathbf{j}$ is the jth line of $\overline{\mathbf{B}}$.

4. Integrated optimization modeling

It is necessary to give an integrated model for actuator placement and control optimization. For truss structures, the locations of active struts can be treated in terms of (0, 1) as discrete variables. Therefore, the integrated optimization can be seen as a nonlinear optimization with mixed variables (discrete and continuous), expressed by how to place p number of actuators on k number of candidate positions to meet the requirements of both the structural-system and the control-system. The integrated optimization model can be written as follows:

$$\begin{aligned}
&\text{Find} \quad \begin{matrix}\mathbf{G} = \{G_1, G_2, \ldots, G_{n_m}\}^\mathrm{T} \\ \boldsymbol{\alpha} = \{\alpha_1, \alpha_2, \ldots, \alpha_{n_c}\}^\mathrm{T}\end{matrix} \\
&\text{Min } \bar{J} = \mathrm{tr}(\mathbf{P}) \\
&\text{s.t. } \overline{\xi}^L \le \xi_i \le \overline{\xi}^U, \quad i = 1,\ldots,n_m \\
&\tau_i \ge \overline{\tau} \\
&n_a \le \overline{n}_a \\
&\alpha_i = 0 \quad \text{or} \quad \alpha_i = 1
\end{aligned} \tag{18}$$

where G is the n_m-dimensional vector of control gain, with n_m number of design variables G_i. α is the n_c-dimensional vector that indicates the presence (1) or absence (0) of the actuator at n_c candidate locations. The quadratic performance index $\bar{J}$ is an objective function. ξ_i, $\overline{\xi}^U$ and $\overline{\xi}^L$ are the closed-loop damping ratio of corresponding mode, its upper limit and its lower limit, respectively. τ_i and $\overline{\tau}$ are the modal controllability and its minimum value. n_a and $\overline{n}_a$ are the actuator number and its allowable number.

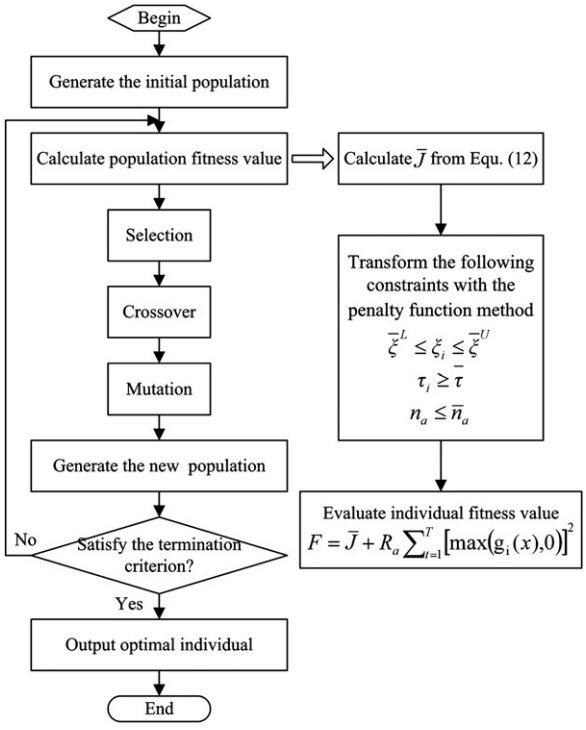

Fig. 1. Flow chart for the integrated optimization solution of adaptive truss.

5. Optimization strategy and algorithm

5.1. Optimization strategy

Layered optimization strategy is employed for the proposed integrated optimization model in (18). The outside-layer GA is applied for the optimization of actuator placement (discrete variable), while the inner-layer LQG algorithm is used for optimal control gain. A flow chart for the integrated optimization solution is shown in Fig. 1.

5.2. Optimization algorithm

The discrete variables of actuator placement are large scale. Thus, to improve computational efficiency, an intelligent optimization algorithm GA is adopted in the outside-layer optimization, which is a guided random search technique simulating natural evolution.

The selection of the genetic operator parameters occurs as follows: (1) a bit string is selected for population type, and its size is 50–100; (2) the rank method is used for fitness scaling; (3) Roulette methods are adapted for the selection; (4) the scattered crossover algorithm is chosen. The reproduction elite count is 2–5, while the crossover fraction is 0.8; and (5) a uniform mutation function is applied, and the rate is 0.01–0.1. Moreover, the GA applies only for unconstrained minimization problems, so a constrained minimization problem should be transformed to an unconstrained one by the penalty function method (see Section 5.3).

In inner-layer continuous optimization, gain G of LQG optimal control is obtained by solving the LQG controller.

5.3. Improvement in penalty function of actuator number constraint

The penalty function method is applied to obtain an unconstrained minimization problem. All constraints can be expressed by $g_i(x) \le 0$. Using the exterior penalty function method, the objective function can be written as

$$F = f + f_a = f + R_a \sum_{t=1}^{T} \left[\max(g_i(x), 0)\right]^2 \tag{19}$$

where F is the penalty function. f is the objective function (viz. $\bar{J}$). f_a is the penalty term. R_a is the penalty factor, which is a relatively large positive number. T is the number of constraints.

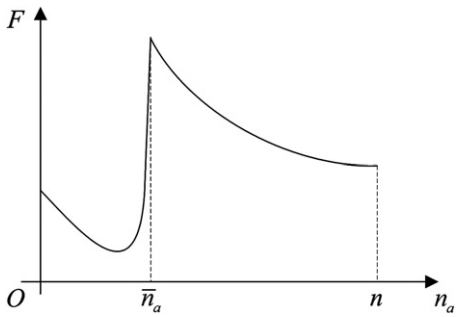

Fig. 2. Relationship between actuator number and penalty function.

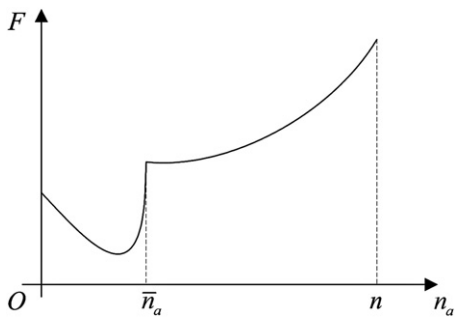

Fig. 3. Relationship between actuator number and improved penalty function.

Outside-layer optimization always contains the actuator number constraint, $n_a \le \overline{n}_a$, thus a penalty term $R_a[\max(n_a - \overline{n}_a, 0)]^2$ always exists. For a complicated truss structure, the strut number n is usually large (i.e., 100). If all struts are candidate positions, the number of possible individuals in the population is 2^n, which is a huge number. The randomly generated initial population is relatively small (i.e., 50–100). Considering that the allowable actuator number is limited (i.e., < 10), and is a small proportion of the whole population, it is very possible that the individuals who satisfy the actuator number constraint are excluded in the initial population. In that case, the penalty function remains large during the optimization and leads to the optimization converging to the local optimal solution, which usually involves all struts being configured with actuators. Here, the relationship between n_a and F is shown in Fig. 2. If the problem is solved by increasing the population number, the computational complexity will significantly increase. Meanwhile, the initial population that randomly generated will induce the problem of stability. However, if this is dealt with by increasing the mutation probability, the GA will degenerate into a random search and rarely find the global optimal solution.

To solve this problem, an improved penalty function for the actuator number constraint is proposed. The penalty term $\overline{f}_a$ is defined

$$\overline{f}_a = R'_a[\max(n_a - \overline{n}_a, 0)]^2 \tag{20}$$

where R'_a is the improved penalty factor, which is expressed as: $R'_a = R_a \cdot n_a$. Using this penalty term, a smaller n_a will produce a smaller F, as shown in Fig. 3. Therefore, the algorithm will orient the population to produce individuals of fewer actuators to satisfy the constraints, and finally arriving at the global optimal solution. The necessity and effectiveness of the improvement are verified in Section 6.2's numerical examples.

6. Numerical examples

6.1. Tri-prism piezoelectric adaptive truss

Optimal actuator placement with LQG control is applied to a tri-prism piezoelectric adaptive truss. The truss is a 2.8-m-long, 11-layer, 102-strut, equilateral triangular cross-section cantilevered boom, as shown in Fig. 4. Nodes 1–3 are fixed on

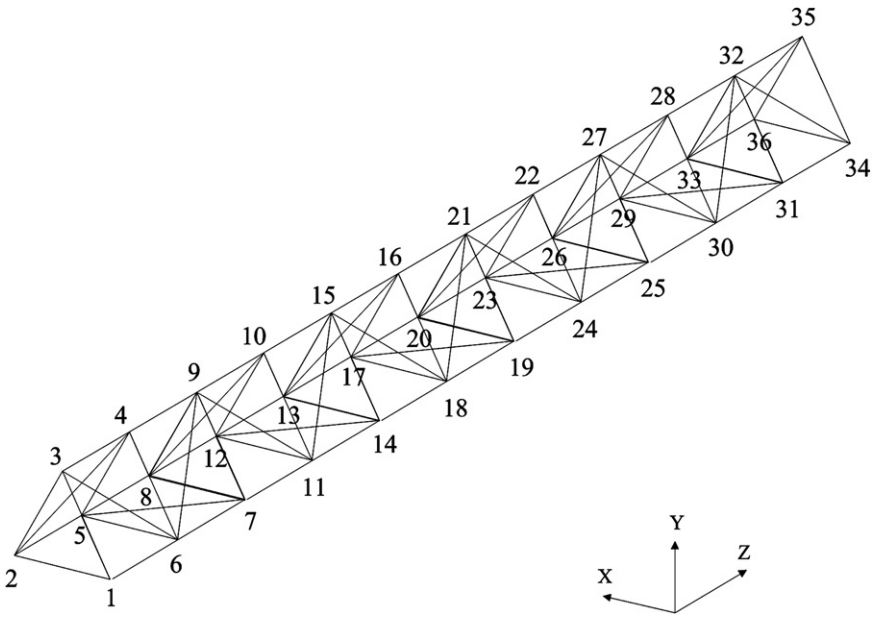

Fig. 4. Model of the adaptive truss.

Table 1
First five modes parameters of the adaptive truss.

Mode	Calculation freq. (Hz)	Mode shape
1	5.2080	1st flexion X
2	5.2088	1st flexion Y
3	20.184	1st torsion Z
4	40.295	2nd flexion X
5	40.378	2nd flexion Y

the base. It is assumed that Young's modulus and the density for both the ordinary strut and the active strut are the same, that is, 1.08×10^{11} Pa and 8940 kg/m^3. The other parameters of the truss are as follows: the equivalent section area is 1.516×10^{-5} m^2, the masses of the nodes and end nodes are 0.135 kg and 1.57 kg, and the actuator expansion coefficient is 0.182 μm V^{-1}. The adaptive truss's calculation frequencies of the first fives modes, obtained from FEM, are shown in Table 1. Sensors 1, 2 and 3 are configured at nodes 19, 26 and 27 with the direction vector of (0.8192, 0.5736, 0), (-0.9397, -0.342, 0) and (0.5, -0.0866, 0), respectively.

In this work, the population scale is 100, and the penalty factor R_a is 50. The weight factor r is 0.05. Compare with the penalty term, the value of $\bar{J}$ is relatively large, hence $\bar{J}$ is reduced 1000 times in the optimization.

6.2. Integrated optimization of first two modes

First two modes of the truss are truncated, while the constraints on the modal damping ratio and the modal controllability are $0.01\leq\ \xi_i\ \leq0.1$ and $\tau_i\geq0.05$, respectively. The number of actuators constraint is $n_a\leq2$. Besides the exciter strut (struts 2–5) and the zero-freedom struts (struts 1–2, 2–3, and 1–3), the remaining 98 struts are selected as candidate locations. As a result, the optimal placements are struts 1–6 and 3–4, while $\bar{J}$ is 1.0968×10^3, the first two modes modal damping ratios are all 0.075, and their modal controllability is 0.488 and 0.311. The corresponding optimal control gain is

$$\mathbf{G}=\begin{bmatrix} 6.2149 & 0.1950 & 5.0645 & -0.8985 \\ -2.9302 & -5.4873 & -1.4397 & -4.9387 \end{bmatrix}$$

The interaction history (plotted in Fig. 5) shows that the penalty function value of the initial population penalty function is very large because of the exclusion of individuals that satisfied the number of actuator constraint. After 20 generations of evolution, individuals that satisfied the constraint are found, the population improved and the value of the penalty function decreased significantly. Finally, an optimal solution is found after approximately 270 generations of evolution. After 20 generations of evolution, the optimal individual's interaction history is locally magnified and plotted in Fig. 6.

Compared with the former optimization, the penalty function value of the population is always large during the interaction history (plotted in Fig. 7) when the original penalty function is adopted, while the corresponding optimal placement involves the remaining 98 struts, which means that the optimization converges to the local optimal solution.

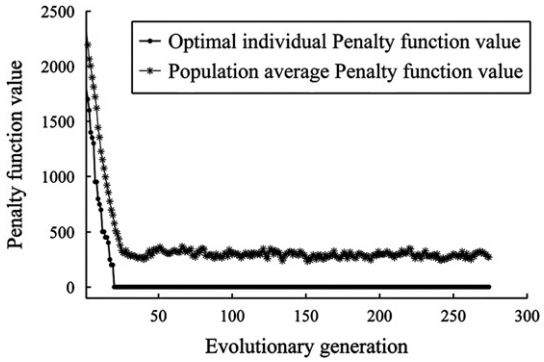

Fig. 5. Interaction history for first two modes.

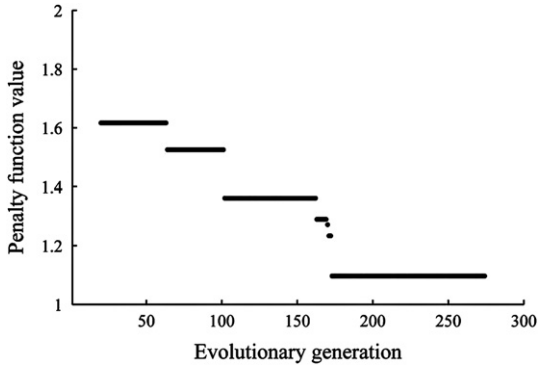

Fig. 6. Local magnified interaction history for first two modes.

6.3. Integrated optimization of first five modes

First five modes of the truss are truncated. To remain consistent with the numerical examples in [7], the number of actuators constraint is set to $n_a \leq 4$. Besides exciter struts (struts 2–4, 2–5 and 18–19) and zero-freedom struts (struts 1–2, 2–3, and 1–3), the remaining 96 struts are selected to be candidate locations. As result, the optimal actuator placements are on struts 1–6, 3–4, 17–20 and 16–21, with $\bar{J}$ equal to 7.7364×10^3. The corresponding optimal control gain is

$$\mathbf{G} = \begin{bmatrix} -4.23 & -0.43 & -52.17 & 58.04 & -45.99 & -4.58 & -0.52 & -1.74 & 4.90 & -0.34 \\ 2.19 & -5.34 & 19.47 & -20.11 & 48.97 & 1.60 & -3.72 & -1.50 & -1.78 & 2.88 \\ 2.26 & 2.64 & -8.15 & 74.48 & 5.44 & 1.82 & 3.01 & 1.93 & 3.31 & 3.13 \\ 3.34 & 3.85 & -26.50 & 11.31 & -63.1 & 1.41 & -2.41 & 1.89 & 2.47 & -3.31 \end{bmatrix}$$

The interaction history (plotted in Fig. 8) shows the same trend as the previous example: the penalty function value of the initial population is very large because individuals that satisfied the number of actuators constraint are not included in

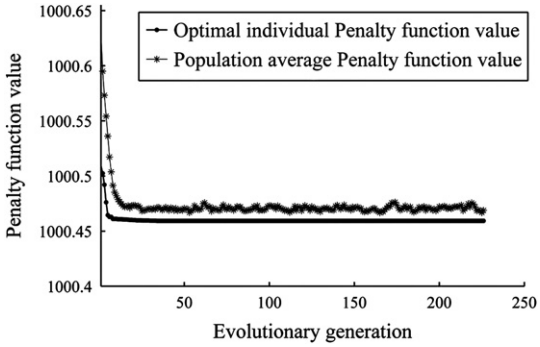

Fig. 7. Interaction history for the first two modes with the original penalty function.

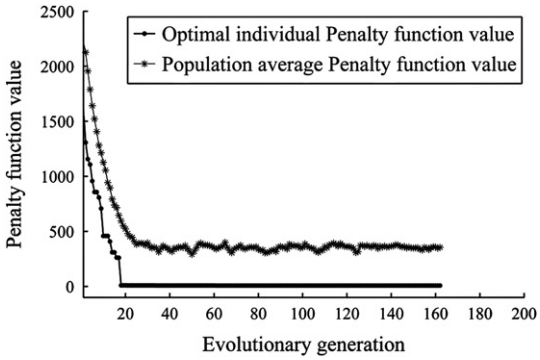

Fig. 8. Interaction history for first five modes.

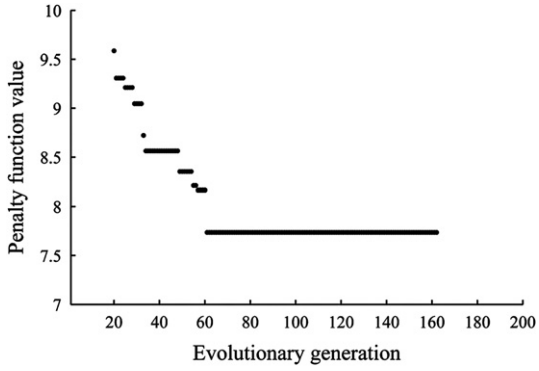

Fig. 9. Local magnified interaction history for first five modes.

Table 2
Computation time for first five modes optimal placement.

Time to compute **G** once	Time to compute the optimal placement
0.0202 s	91.6452 s

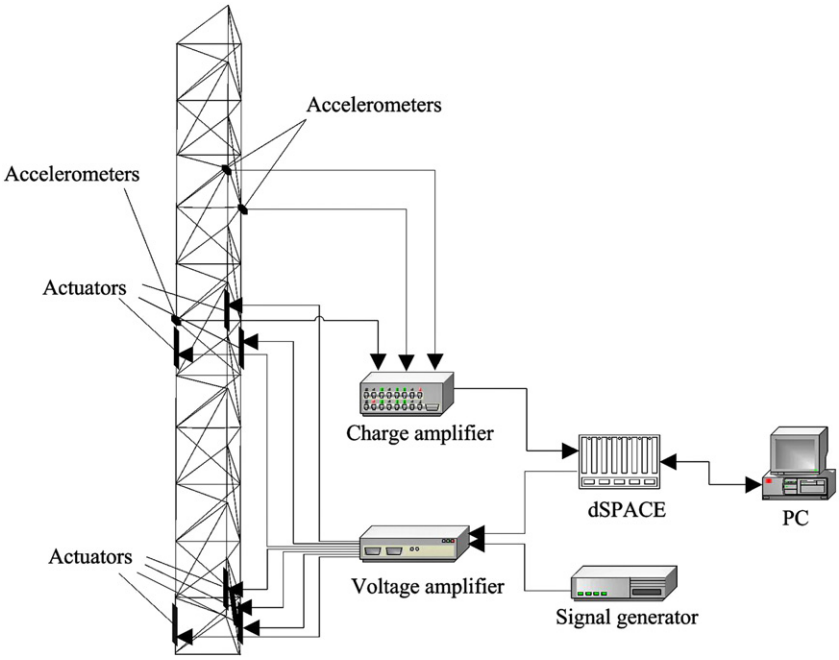

Fig. 10. Schematic graph of the piezoelectric adaptive truss test-bed.

the initial population. However, after 20 generations of evolution, searching is conducted within the group of individuals who satisfied the constraint, and the optimal solution is found after approximately 160 generations of evolution. After 20 generations of evolution, the optimal individuals' interaction history is locally magnified and plotted in Fig. 9.

The optimization computation was executed on a PC with a 1.83 GHz Intel CPU, 512 MB of memory and Windows XP OS. The computation time of the example, listed in Table 2, shows that although the number of struts is large, the computation takes a relatively short amount of time. The reasons for this are as follows: (1) the computation speed of the LQG optimal control gain **G** is fast. (2) The structure mass and stiffness matrix (**M** and **K**) are assembled only once during the optimization because of the consistency assumption for the mass and stiffness of ordinary strut elements and active strut elements. (3) The control force vector ($\mathbf{L}_{\mathbf{v}}^{\mathbf{e}}$) is solved only once but can be called at any time.

For the same example, the optimal actuator placement in paper [7] includes struts 1–6, 3–4, 19–24 and 21–22, while $\bar{J}$ is 8.6785×10^3 which is worse than the result in the present paper. Experiments were conducted to compare these two kinds of optimal actuator placements.

7. Vibration control experiment

7.1. Piezoelectric adaptive truss test-bed

A schematic graph and a photograph of the experimental setup for a piezoelectric adaptive truss test-bed are displayed in Figs. 10 and 11. The truss geometry and material parameters are identified in Section 6.1.

There are two piezoceramic stack actuators that were designed and manufactured by us, PZT-1 and PZT-3, which were installed at the bottom of the truss and on the middle struts, respectively. Their geometries are $\Phi 28$ mm $\times$ 190 mm and $\Phi 20$ mm $\times$ 120 mm, their masses are 482 g and 80 g, the dynamic piezo expansion coefficients are 0.182 μm/V and 0.415 μm/V, and the dynamic force constants are 1.25 N/V and 0.78 N/V.

The controller was designed using Matlab/Simulink and downloaded to the processor of the dSPACE DS1005 real-time control/simulation system. The truss response is measured by *Sinocera Piezotronics Inc.* CA-YD-139 single-axis piezoelectric accelerometers, whose axial sensitivity, frequency response and shock limit are 1.2 pC/m s^{-2}, 0.3–3 kHz and

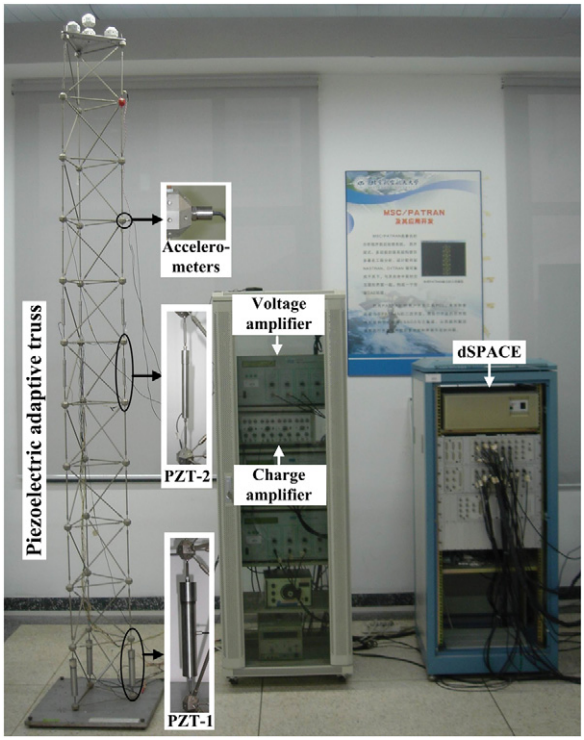

Fig. 11. Experimental setup of the piezoelectric adaptive truss test-bed.

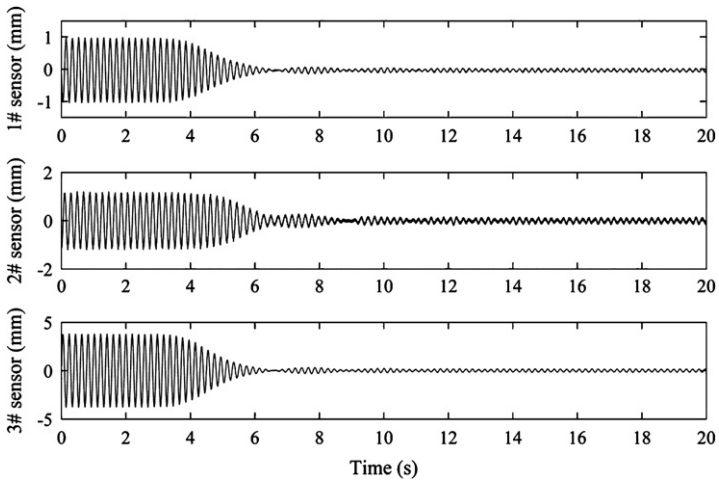

Fig. 12. Time response of sensors with actuator placement at struts 1–6 and 3–4 (optimal placement).

1×10^4 m s^{-2}, respectively. The accelerometers' signals are received from the charge amplifier via an AD converter. The dSPACE DS1005 then processes this signal and generates a command, which is sent to the 260 V/150 W DC linear voltage amplifier through a DA converter. Both the AD converter and the DA converter are hardware components of the DS1005 system.

7.2. Vibration control of first two modes

First two mode's experiments were carried out for three kinds of actuator placements. In addition to the present paper's optimal placement (struts 1–6 and 3–4), the other two placements, struts 1–6/16–21 and struts 1–6/2–4, are the locations where the strain energy of the first two modes is relatively large. In the experiment, the sinusoidal disturbance of the first two modes frequency is produced by struts 2–5. After the disturbance becomes balanced, each controller is called out, and

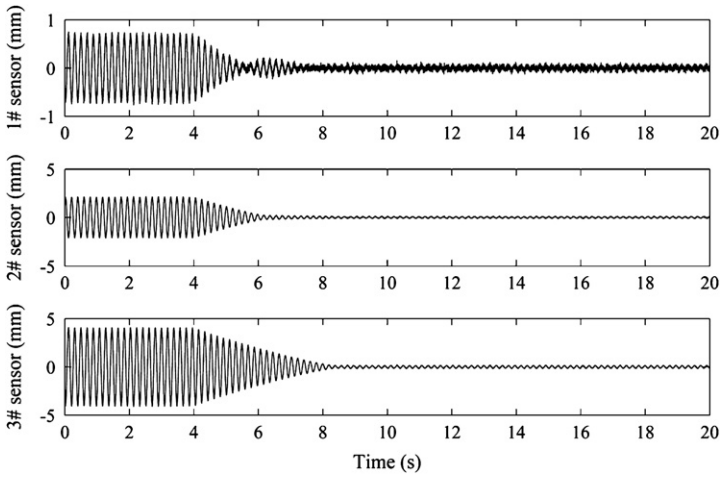

Fig. 13. Time response of sensors with actuator placement at struts 1–6 and 3–4, in numerical simulation.

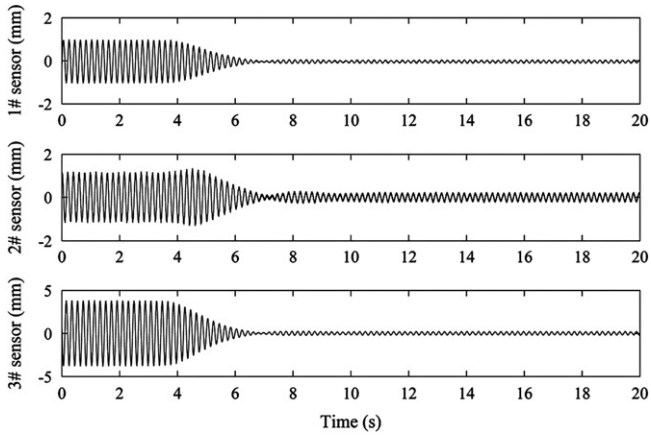

Fig. 14. Time response of sensors with actuator placement at struts 1–6 and 16–21.

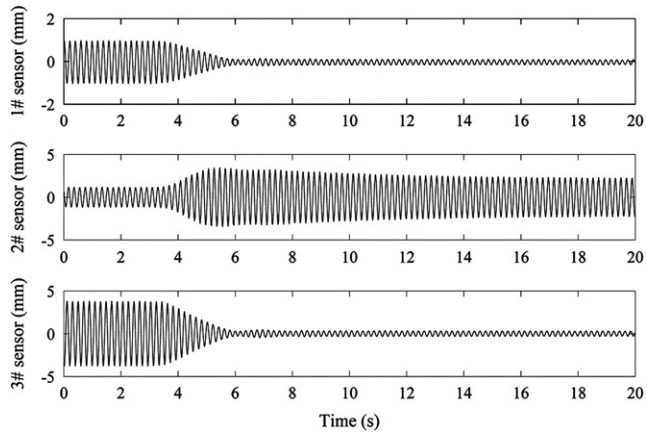

Fig. 15. Time response of sensors with actuator placement at struts 1–6 and 2–4.

the time responses of the sensors and the corresponding modal coordinates are shown in Figs. 12 and 14–18, respectively. Fig. 13 is the time response of sensors with optimal placement in numerical simulation. To simulate the practical situation, Gaussian white noise, which mean and variance are 0 mm and 0.001 mm, is added to observation function in the model. Compared with Fig. 12, because of the modeling errors and disturbance amplitude errors, the vibration amplitudes are not

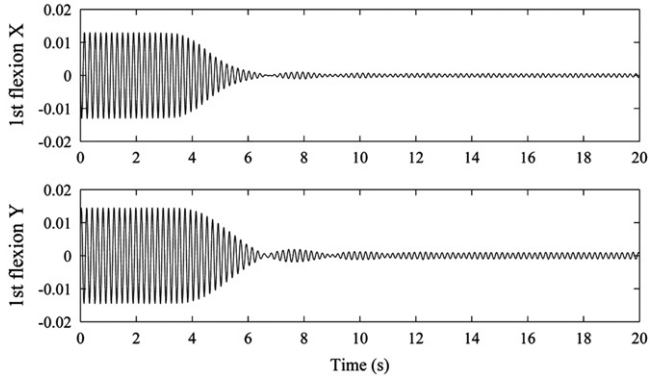

Fig. 16. Time response of the modal coordinates with actuator placement at struts 1–6 and 3–4 (optimal placement).

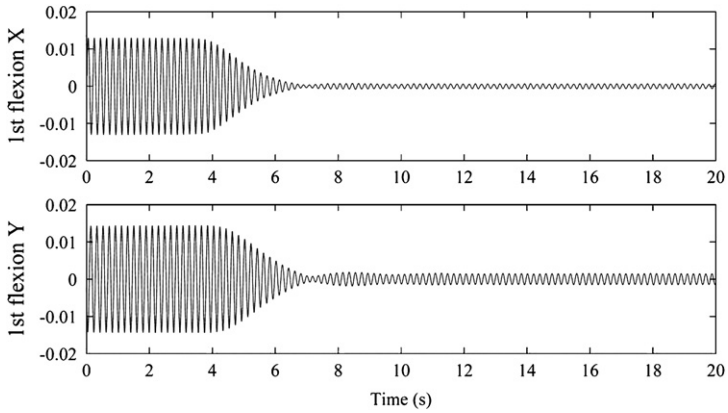

Fig. 17. Time response of the modal coordinates with actuator placement at struts 1–6 and 16–21.

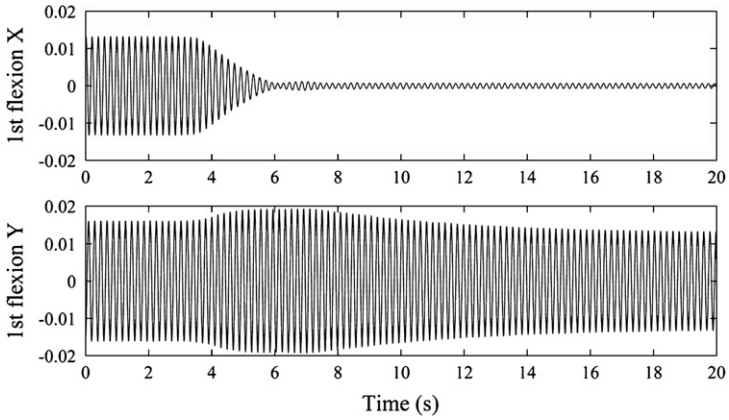

Fig. 18. Time response of the modal coordinates with actuator placement at struts 1–6 and 2–4.

Table 3
Two-order model quadratic performance for different placements.

Placement	$\bar{J}$	J
Struts 1–6 and 3–4 (optimal placement)	$\mathbf{1.0968 \times 10^3}$	**2.2424**
Struts 1–6 and 16–21	1.3616×10^3	2.4394
Struts 1–6 and 2–4	3.7876×10^3	7.2885

completely consistent, but their average reductions rates of three sensors (91.6 percent in the numerical simulation and 90.6 percent in experiment) are very close. That means the control abilities of experimental and numerical simulation are the same.

The quadratic performance index for three kinds of actuator placements are listed in Table 3, in which J is calculated by numerically integrating the experimental data under the same initial conditions. The values and magnitude of $\bar{J}$ and J are different because of the different calculation methods, but the monotonicity and trend are consistent, which proves the rationality of replacing the objective function J by $\bar{J}$, which was described in Section 3.2.

The experimental results of first two modes show that compared with two other actuator placements, the quadratic performance index of the optimal placement is the best.

7.3. Vibration control of first five modes

First five modes experiments were conducted for both the present paper's and paper [7]'s optimal placement. In the experiment, the sinusoidal disturbance of the first five modes frequency is produced by struts 2–5, 2–4 and 18–19. After the disturbance becomes balanced, the controller is called out. The response times of the sensors and the corresponding modal coordinates are shown in Figs. 19, and 21–23, respectively. Fig. 20 is the time response of sensors with the present paper's placement in numerical simulation. Gaussian white noise, which mean and variance are 0 mm and 0.001 mm, is added to observation function. Compare with Fig. 19, the same conclusion can be obtained as first two modes control. The average reduction rates of three sensors (83.4 percent in the numerical simulation and 80.5 percent in experiment) are close, too.

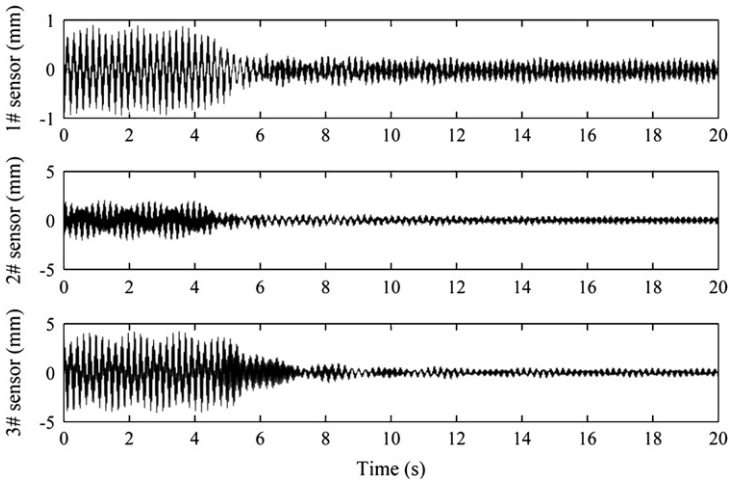

Fig. 19. Time response of the sensors with actuator placement of the present method.

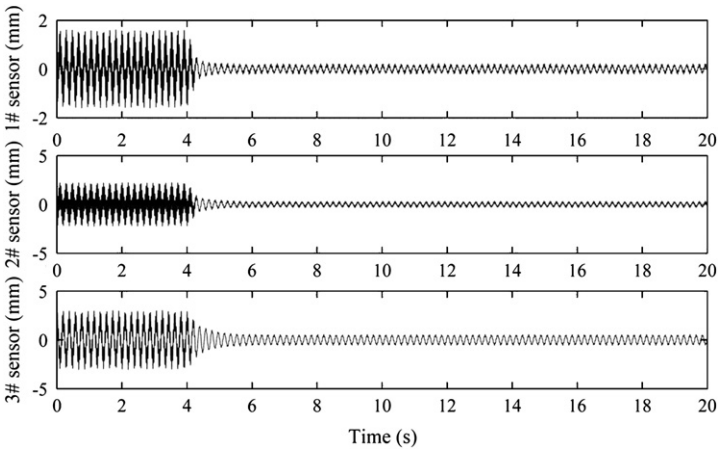

Fig. 20. Time response of the sensors with actuator placement of the present method in numerical simulation.

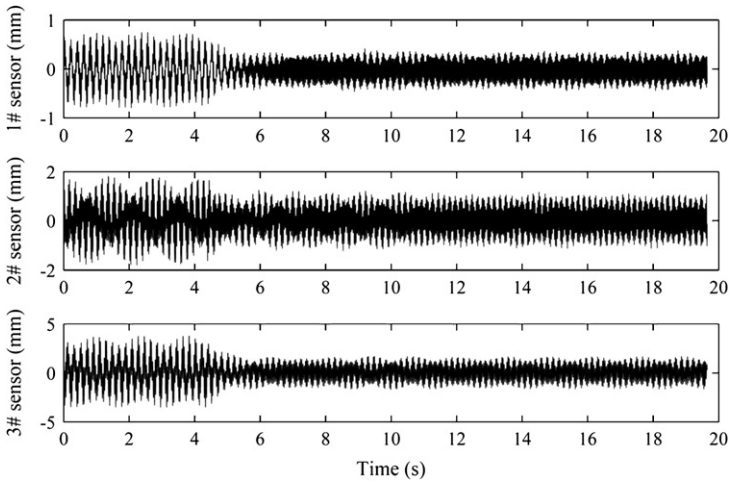

Fig. 21. Time response of the sensors with actuator placement of paper [7].

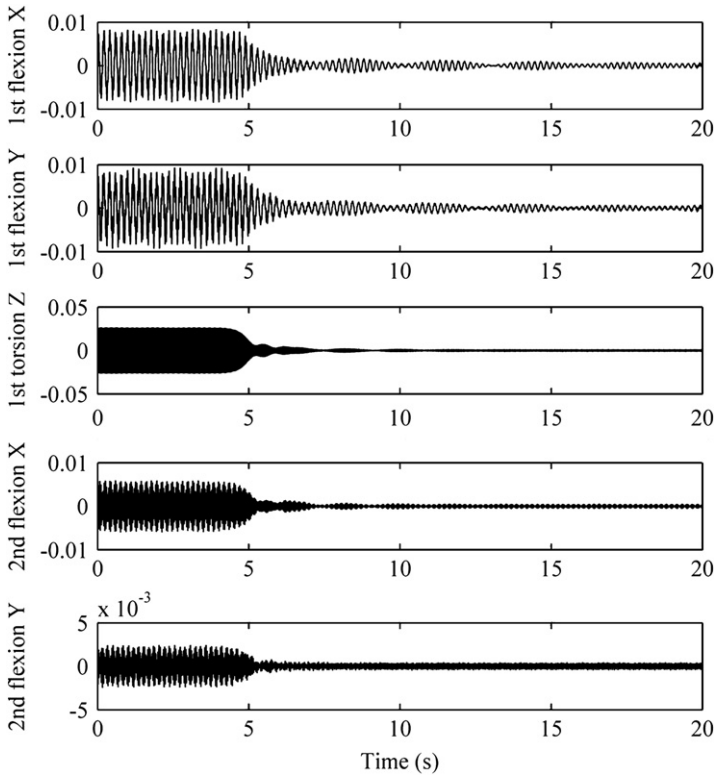

Fig. 22. Time response of the modal coordinates with actuator placement of the present method.

The quadratic performance index, the modal response and the control energy for two kinds of actuator placements are listed in Table 4. J_1 and J_2 were calculated by numerical integration of the modal coordinate and control voltage experimental data.

The experimental results show that (1) the sensor signals and modal displacements of the present paper's optimal placement are superior to those of paper [7], especially for high-order modes; that (2) for actuators that were placed in locations where the truss higher mode deformation energy is relatively large, the actuator voltages for the present paper's optimal placement are significantly larger than those of paper [7], that is, excellent control of the truss's higher modes required more energy; and that (3) quadratic performance of the present paper's optimal placement is better than that of paper [7], which shows the effectiveness of integrated optimization.

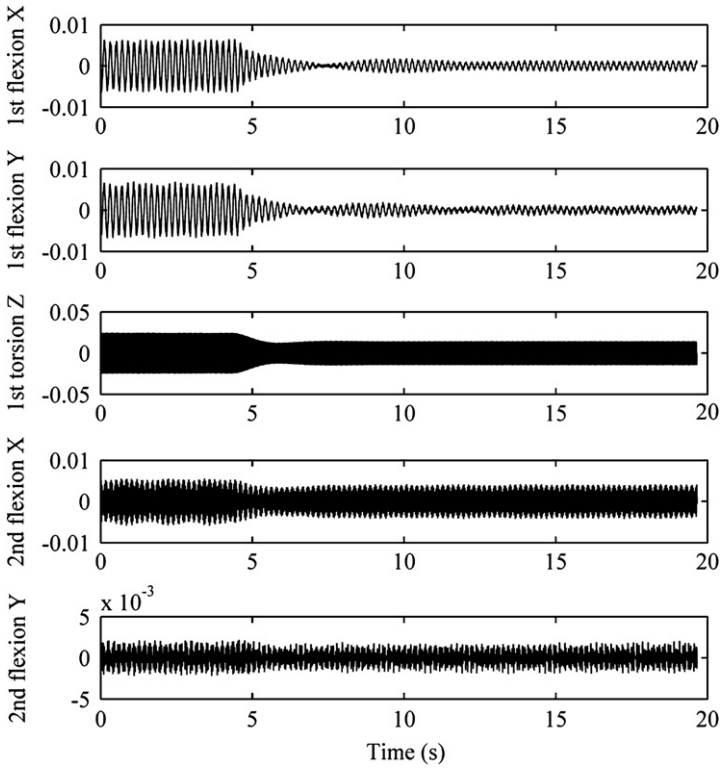

Fig. 23. Time response of the modal coordinates with actuator placement of paper [7].

Table 4
Five-order model quadratic performance with different actuator placements.

Placement	$\bar{J}$	J	Mode response $J_1 = \int \mathbf{X}^{\mathrm{T}}\mathbf{Q}\mathbf{X}\,\mathrm{d}t$	Control energy $J_2 = \int \mathbf{V}^{\mathrm{T}}\mathbf{R}\mathbf{V}\,\mathrm{d}t$
Present paper's placement	7.7364×10^3	15.100	12.812	2.288
Paper [7]'s placement	8.6785×10^3	15.411	14.703	0.708

8. Conclusion

In this paper, integrated optimization of actuator placement and vibration control for a piezoelectric adaptive truss was studied. To solve this optimization problem with discrete-continuous design variable, a layered optimization strategy was used. The penalty function in the outside-layer GA optimization was improved. The numerical results show the effectiveness of the improved penalty function and the computational efficiency of the proposed method. Moreover, in the experiment, the control effect and the quadratic performance index of the present paper's actuator placement were better than another placement published in the literature, which was consistent with the numerical results.

Acknowledgements

The authors would like to acknowledge the support of the China Aerospace Science and Technology Corporation under the Grant of CASC200902 and the China Academy of Space Technology under Grant CAST20100601.

References

[1] K. Miura, H. Furuya, Adaptive structure concept for future space applications, *AIAA Journal* 26 (8) (1988) 995–1002.
[2] B.K. Wada, Adaptive structures, *Journal of Spacecraft and Rocket* 27 (3) (1990) 330–337.
[3] J.A. Garba, B.K. Wada, J.L Fanson, Adaptive structures for precision controlled large space systems, *Journal of Intelligent Material System & Structures* 3 (2) (1992) 348–366.
[4] E.F. Crawley, Intelligent structures for aerospace: a technology overview and assessment, *AIAA Journal* 32 (8) (1994) 1689–1699.
[5] R.A. Manning, Optimum design of intelligent truss structures. Proceedings of the 32nd AIAA/ASME/ASCE/AHS/ASC Structures, Structural Dynamics and Materials Conference, Baltimore, April 1991, pp. 528–533.

[6] W. Gao, Stochastically optimal active control of a smart truss structure under stationary random excitation, *Journal of Sound and Vibration* 290 (2006) 1256–1268.
[7] K.C. Xian, Optimal actuators locations for adaptive structures and structure optimization including discrete variables, PhD Thesis, Beihang University, Beijing, 2007.
[8] S. Liu, Z. Lin, Integrated design optimization of voltage channel distribution and control voltages for tracking the dynamic shapes of smart plates, *Smart Materials and Structures* 19 (2010) 125013.
[9] S.S. Rao, V.B. Venkayyat, N.S. Khotf, Game theory approach for the integrated design of structures and controls, *AIAA Journal* 26 (4) (1988) 463–469.
[10] K. Xu, P. Warnitchai, T. Igusa, Optimal placement and gains of sensors and actuators for feedback control, *Journal of Guidance Control and Dynamics* 17 (5) (1994) 929–934.
[11] G. Zhao, B. Chen, Y. Gu, Control–structural design optimization for vibration of piezoelectric intelligent truss structures, *Structural and Multidisciplinary Optimization* 37 (2009) 509–519.
[12] Y. Yang, Zhi Jin, C.K. Soh, Integrated optimal design of vibration control system for smart beams using genetic algorithms, *Journal of Sound and Vibration* 282 (2005) 1293–1307.
[13] B. Xu, J.S. Jiang, J.P. Ou, Integrated optimization of structural topology and control for piezoelectric smart trusses using genetic algorithm, *Journal of Sound and Vibration* 307 (2007) 393–427.
[14] S. Honda, I. Kajiwara, Y. Narita, Multidisciplinary design optimization for vibration control of smart laminated composite structures, *Journal of Intelligent Material Systems and Structures* 22 (13) (2011) 1419–1430.
[15] R. Dutta, R. Ganguli, V. Mani, Swarm intelligence algorithms for integrated optimization of piezoelectric actuator and sensor placement and feedback gains[J], *Smart Materials and Structures* 20 (2011) 105018.
[16] A.E. Sepulveda, L.A. Schimit, Optimal placement of actuators and sensors in control-augmented structural optimization, *International Journal for Numerical Methods in Engineering* 32 (1991) 1165–1187.